Vol 465|13 May 2010|doi:10.1038/nature09057

ARTICLES

Single-molecule dynamics of gating in a neurotransmitter transporter homologue

Yongfang Zhao[1,2,3]*, Daniel Terry[4]*, Lei Shi[4,5], Harel Weinstein[4,5], Scott C. Blanchard[4] & Jonathan A. Javitch[1,2,3,6]

Neurotransmitter:Na^+ symporters (NSS) remove neurotransmitters from the synapse in a reuptake process that is driven by the Na^+ gradient. Drugs that interfere with this reuptake mechanism, such as cocaine and antidepressants, profoundly influence behaviour and mood. To probe the nature of the conformational changes that are associated with substrate binding and transport, we have developed a single-molecule fluorescence imaging assay and combined it with functional and computational studies of the prokaryotic NSS homologue LeuT. Here we show molecular details of the modulation of intracellular gating of LeuT by substrates and inhibitors, as well as by mutations that alter binding, transport or both. Our direct observations of single-molecule transitions, reflecting structural dynamics of the intracellular region of the transporter that might be masked by ensemble averaging or suppressed under crystallographic conditions, are interpreted in the context of an allosteric mechanism that couples ion and substrate binding to transport.

The neurotransmitter:Na^+ symporter (NSS) family stops cellular signalling by recapturing released neurotransmitter[1–3]. These secondary active transporters enable the thermodynamically uphill transport of their substrates across the plasma membrane of the presynaptic neuron in a co-transport (symport) mechanism driven by the Na^+ electrochemical gradient[4–6]. The transporters for the biogenic amines, dopamine, noradrenaline and serotonin, are of particular interest because they are targeted by numerous drugs, including antidepressants[7] and the widely abused psychostimulants cocaine and amphetamine[1]. Genes that encode more than 200 putative NSS homologues have been identified in prokaryotic genomes[8]. The crystal structure of LeuT[9], a prokaryotic NSS homologue from the thermophile *Aquifex aeolicus* that comprises 12 transmembrane (TM) helices, revealed an occluded state in which one leucine and two Na^+ ions are bound deep within the protein (Fig. 1). When reconstituted into proteoliposomes, LeuT mediates Na^+-dependent transport of leucine and alanine at rates of ~0.1–0.4 molecules per min[10]. Computational and experimental studies identified a key mechanistic role for a second substrate binding site in the extracellular vestibule, comprising many of the residues that interact with antidepressants[10–13]. The two binding sites can be occupied simultaneously, and substrate in the second (S2) site allosterically triggers intracellular release of Na^+ and substrate from the primary (S1) site[10]. By contrast, tricyclic antidepressants (TCAs), which also bind in the S2 site (Fig. 1), do not promote substrate release from the S1 site. Instead, TCAs competitively block substrate binding to the S2 site and inhibit transport. Thus, the allosteric changes in LeuT that are induced by substrate binding to the S2 site must differ from those, if any, produced by binding of TCAs.

Notably, the crystal structures of LeuT with and without TCA bound are almost identical. Moreover, so far all LeuT structures have been solved in the detergent *n*-octyl-β-D-glucopyranoside (OG)[9,11,12,14], whereas functional studies of LeuT have been carried out with protein purified in the detergent *n*-dodecyl-β-D-maltopyranoside (DDM)[9–12,14]. Like TCAs, OG competes with substrate binding to the S2 site and disrupts the Na^+-coupled symport mechanism[15]. Thus, all available LeuT structures are likely to represent functionally blocked states in which allosteric changes related to function might be difficult or impossible to discern.

To investigate the nature of the conformational changes that are associated with substrate binding and transport, we used an integrated approach including functional, computational and single-molecule fluorescence imaging techniques. We used single-molecule

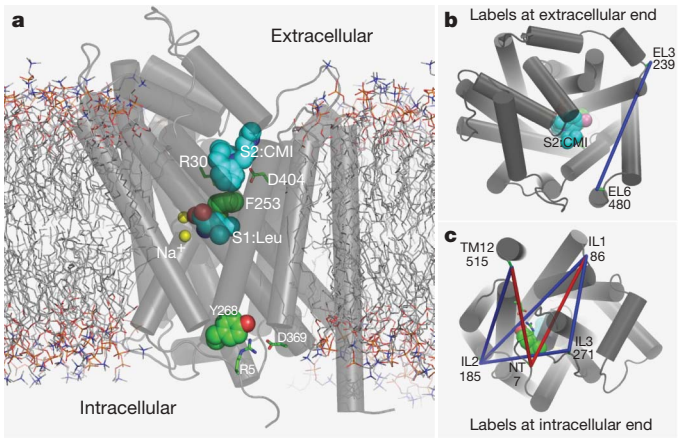

Figure 1 | Structural landmarks and the disposition of the engineered Cys pairs in the crystal structure of LeuT. a, Side view of the LeuT crystal structure equilibrated in a POPC lipid bilayer, showing Leu in the S1 site, CMI in the S2 site, sodium ions as yellow spheres and the surrounding lipid molecules in thin stick rendering. The intracellular surface is at the bottom. Residues involved in conserved ionic:cation-π interactions in both the putative extracellular and intracellular gates are shown in volume rendering. **b, c**, The Cys pairs used to monitor rearrangements at the extracellular (**b**) and intracellular (**c**) ends of the transporter, under designated conditions.

[1]Center for Molecular Recognition, Columbia University College of Physicians and Surgeons, 630 W. 168th, New York, New York 10032, USA. [2]Departments of Psychiatry, Columbia University College of Physicians and Surgeons, 630 W. 168th, New York, New York 10032, USA. [3]Division of Molecular Therapeutics, New York State Psychiatric Institute, New York, New York 10032, USA. [4]Department of Physiology and Biophysics, Weill Cornell Medical College, 1300 York Avenue, New York, New York 10021, USA. [5]HRH Prince Alwaleed Bin Talal Bin Abdulaziz Alsaud Institute for Computational Biomedicine, Weill Cornell Medical College, 1300 York Avenue, New York, New York 10021, USA. [6]Department of Pharmacology, Columbia University College of Physicians and Surgeons, 630 W. 168th, New York, New York 10032, USA.
*These authors contributed equally to this work.

fluorescence resonance energy transfer (smFRET) methods to observe and quantify time-dependent changes in LeuT structure, which could be masked by ensemble averaging in bulk measurements or suppressed through crystallographic conditions[16–28]. We assessed the mechanistic context of the observed conformational changes in LeuT computationally using molecular dynamics simulations related to the functional assays[10,15,29–33]. Here, we focused on understanding conformational events on the intracellular side of LeuT, as large conformational changes in this region have not been revealed through crystallographic means but are required for inward substrate release.

We performed single-molecule experiments on single and double cysteine LeuT mutants that were linked to fluorophores through maleimide chemistry. Cysteine residues were introduced into LeuT, which lacks native cysteines, at non-conserved positions. Crystal structures and molecular dynamics simulations showed that these positions were distal to the established ligand binding sites and accessible to solvent. We selected LeuT mutants for investigation on the basis of efficient fluorophore coupling (>80–90%) and low nonspecific labelling (<4%) (Supplementary Fig. 1), low anisotropy parameters (Supplementary Table 1) and wild-type-like proteoliposome-reconstituted transport activity (Supplementary Table 2). These criteria identified six cysteine pairs on the intracellular side of the transporter that were suitable for imaging experiments. These included combinations of cysteine substitutions for His 7 in the amino terminus (NT), Arg 86 in intracellular loop (IL)1, Arg 185 in IL2, Lys 271 in IL3 and Thr 515 at the cytoplasmic end of TM12. To obtain comparative measures of motion, we also selected one cysteine pair (positions Lys 239 in extracellular loop (EL)3 and His 480 in EL6) on the extracellular surface of LeuT (Fig. 1).

We initially performed smFRET experiments on N-terminally His-tagged, Cy3/Cy5-labelled LeuT in 0.03% DDM, surface immobilized through a biotin–NTA interaction in passivated, streptavidin-coated microfluidic chambers[34,35] (Fig. 2 and Supplementary Fig. 2). By controlling the density of surface immobilization through dilution and using a prism-based, wide-field configuration, we could simultaneously image low-density arrays of specifically tethered, individual LeuT molecules. We achieved oxygen scavenging and triplet state quenching conditions for optimal fluorophore performance (low photophysical noise and reduced photobleaching) through screening[36] (see Methods). Initial measurements of H7C/R86C- and H7C/T515C-labelled LeuT molecules, performed at 40 ms time resolution and high signal-to-noise ratio (~18:1 on average), showed that both systems, in the presence of 200 mM K^+ and the nominal absence of Na^+, displayed two readily distinguished FRET states (~0.51 and ~0.75; ~0.43 and ~0.73, respectively; Fig. 2b, c and Supplementary Fig. 3). These observations indicated that there might be two distinct LeuT conformations in the population differing by ~13 Å in the distance between each fluorophore pair (Supplementary Table 3).

Consistent with the half-maximum effective concentration (EC_{50}) of Na^+ for stimulating binding and transport (~10 mM)[10], and a ligand-dependent transition between these states, the relative populations of low- and high-FRET LeuT conformations depended on Na^+ concentration. Addition of saturating Na^+ concentrations (200 mM) stabilized higher-FRET states in both systems (~0.77 and ~0.73, for H7C/R86C and H7C/T515C, respectively; Fig. 2, Supplementary Table 3 and Supplementary Fig. 3), consistent with substrate-bound LeuT crystal structures, in which the intracellular end of the transporter is compact[9,14]. High-FRET state occupancy was saturated at 200 mM Na^+. Under such conditions, we did not observe further changes in FRET on addition of 20 μM leucine (Fig. 2c and Supplementary Table 3). However, at 5 mM Na^+, where both low- and high-FRET states remain populated, leucine binding redistributed the two populations in a concentration-dependent fashion in favour of higher-FRET configurations (Fig. 2d. The same results were obtained whether LeuT molecules were immobilized by the N terminus or the C terminus).

These findings are consistent with spontaneous, ligand-modulated rearrangements in specific elements of LeuT near the intracellular gating region. In the absence of ligands, a low-FRET state would be achieved by an outward and/or downward movement of position 7 (at the N terminus of TM1) with respect to positions 86 (IL1) and 515

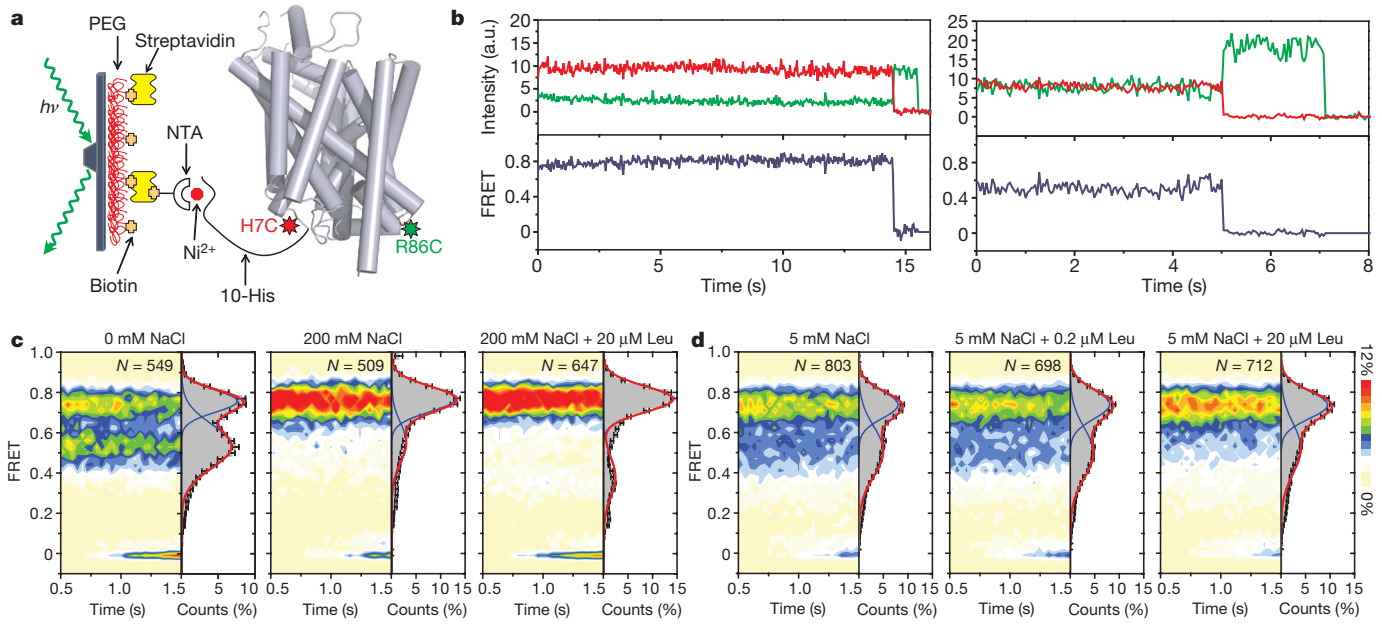

Figure 2 | Single-molecule imaging of LeuT. **a**, His-tagged, dye-labelled LeuT-H7C/R86C was immobilized by biotin-NTA-Ni^{2+} to the streptavidin-treated surface. **b**, Representative fluorescence (Cy3 donor in green, Cy5 acceptor in red) and FRET (grey) time traces from experiments in 200 mM KCl. **c**, FRET traces were summed into histograms in 200 mM KCl (left), 200 mM NaCl (centre), and 200 mM NaCl with 20 μM leucine (right). Each two-dimensional histogram was summed over time (grey bars, on side), filtered to remove fluorophore dark states (see Methods), and fit to the sum (red) of two Gaussian distributions (blue) to estimate the mean value and relative occupancies of each FRET state. **d**, Histograms are shown for experiments performed in 5 mM NaCl with no substrate (left), 200 nM leucine (centre) and 20 μM leucine (right). Scale on right indicates the relative population.

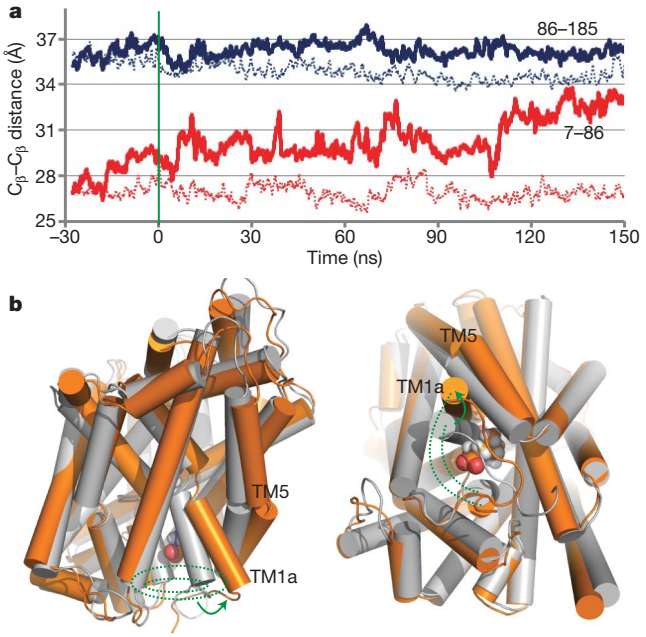

Figure 3 | The structural context of the observed dynamic changes. **a**, Evolution of distances between cysteine pairs (the distance between the C_β atoms of two residues, C_β–C_β distances) for specific residues (numbers at right-hand end of traces) observed in molecular dynamics simulations in the absence (dotted lines) and presence (solid lines) of simulated transport. **b**, Superposition of snapshots from the molecular dynamics equilibrations of the crystal structure of LeuT (grey) and the inward-open structure (orange) indicating the conformational rearrangements predicted from the molecular dynamics simulations in the transport mechanism (see Supplementary Movies 1 and 2). In this molecular dynamics frame, the descending leucine substrate is shown near the site of intracellular opening, where the proposed TM1a rearrangement is indicated by arrows. The left and right panels show views parallel to the membrane and from the intracellular side, respectively. The dotted lines comprising the intracellular ends of the same TMs that surround the exiting substrate in the open-inward structure obtained through simulation (orange) yield a larger circumference than in the crystal structure (grey).

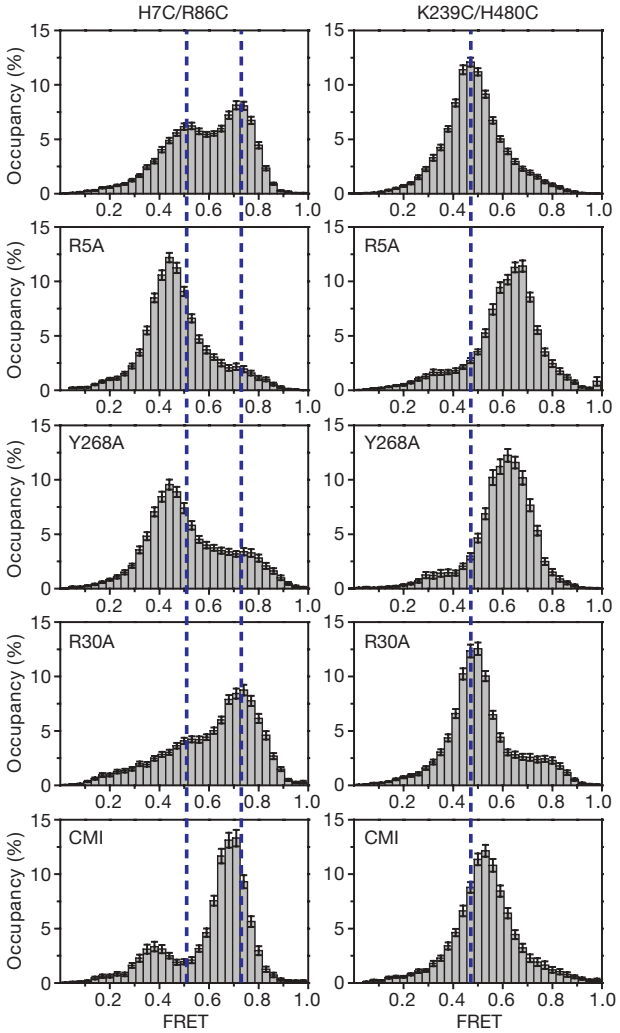

Figure 4 | Effects of mutation and CMI on FRET histograms of LeuT-H7C/R86C and LeuT-239C/480C. FRET histograms from single-molecule traces obtained in the presence of 200 mM KCl for LeuT-H7C/R86C (left) and LeuT-239C/H480C (right) are shown in the context of the mutations R5A, Y268A or R30A, or the presence of 0.5 mM CMI. For clarity, fluorophore dark states have been computationally removed from all histograms (see Methods). Error bars are the standard deviation of 1,000 bootstrap samples of the FRET traces.

(cytoplasmic end of TM12). Correspondingly, a high-FRET state could be achieved spontaneously or upon ligand binding by a reciprocal motion of TM1 with respect to IL1 and TM12, leading to an inward-closed LeuT conformation. By contrast, we observed no substrate-dependent changes for any of the other constructs labelled on the intracellular face of the protein (Supplementary Fig. 4), indicating that these positions do not move substantially during intracellular gating.

The site of labelling at position 7 is adjacent to the highly conserved Trp 8 residue, which is involved in a conserved interaction network among a residue triad that includes Ile 187 (IL2) and Tyr 268 (IL3) at the intracellular face (Supplementary Fig. 5)[32]. Tyr 268 also forms cation-π and ionic interactions with residues Arg 5 (at the N terminus) and Asp 369 (TM8), thereby bringing together NT, IL2 and IL3 and closing the transport pathway at the intracellular surface of LeuT (Fig. 1). Mutation of the homologous interaction network in the structurally related dopamine transporter and GABA transporter has been inferred to promote inward-open conformations[32,37].

To interpret the distance changes identified with smFRET with respect to changes occurring in the intracellular interaction network during the transition from an outward-open to an inward-open conformation, and to investigate how they might pertain to the transport mechanism, we performed molecular dynamics simulations. Inward-open conformations of LeuT generated by computationally 'pulling' the S1 site-bound substrate intracellularly in the presence of S2 and the absence of Na2 (ref. 10), were subjected to prolonged MD simulations (two parallel runs of 150 ns each), designed to examine the structural equilibration of LeuT after the simulated substrate transport event. During the extended equilibration period, we observed dissociation of the Trp 8–Ile 187–Tyr 268 interaction network. This resulted in a relative downward and outward movement of TM1 and the region containing the residue at position 7, and a corresponding increase in the distance between positions 7 and 86 (Fig. 3 and Supplementary Movies 1 and 2) and position 7 and the intracellular end of TM12 (Supplementary Fig. 6). This rearrangement was associated with significant conformational changes in the IL2–TM5 region (including Ile 187), facilitated by changes in the bend angle of the highly conserved proline kink in TM5. By contrast, the distance between residues 86 and 185 was largely unchanged throughout the simulation (Fig. 3) as the bottom of TM4 maintained a relatively stable position.

We therefore found that the conformational rearrangements in LeuT observed during the simulated transport event leading to the inward-open conformation agreed well with the estimated changes in distance deduced from the smFRET data. A recent analysis of crystal structures sharing a LeuT-like fold prompted Gouaux and colleagues to propose that coordinated rearrangements of TM1a and TM1b are associated with conformational transitions in the protein[38]. Both our

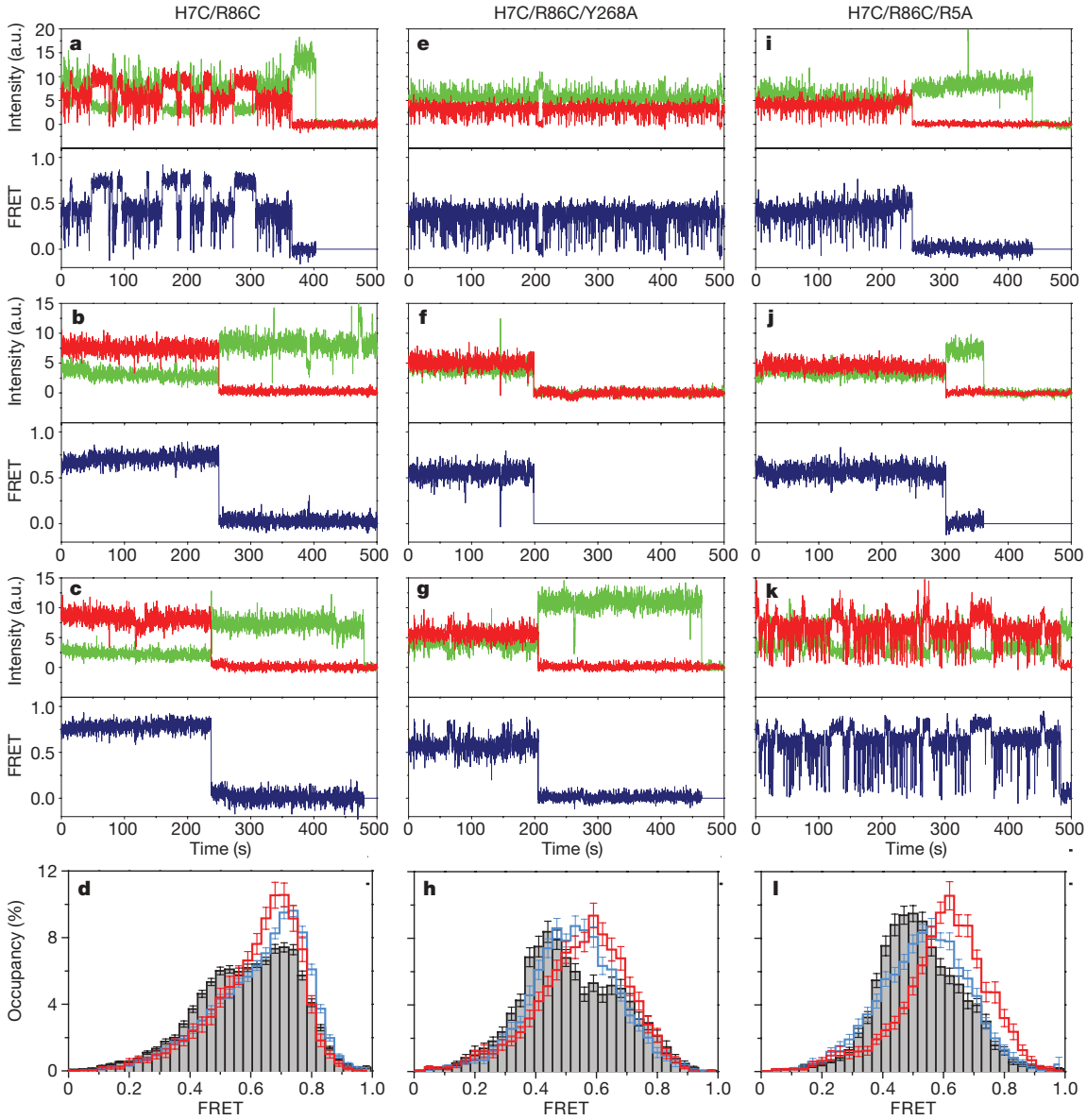

Figure 5 | Long single-molecule trajectories reveal FRET transitions. Representative single-molecule traces from 160-ms images are shown for LeuT-H7C/R86C (left), LeuT-H7C/R86C/Y268A (centre), and LeuT-H7C/R86C/R5A (right) in 200 mM KCl (**a**, **e**, **i**), 200 mM NaCl (**b**, **f**, **j**) or 200 mM NaCl and 20 μM leucine (**c**, **g**, **k**). Cy3 (donor) and cy5 (acceptor) fluorescence are shown in green and red, respectively. FRET efficiency is shown in blue. One-dimensional histograms (**d**, **h**, **l**) represent the population data obtained in the presence of 200 mM KCl (grey bars), 200 mM NaCl (blue line), or 200 mM NaCl and 20 μM leucine (red line). Error bars are the standard deviation of 1,000 bootstrap samples of the FRET traces.

simulation and smFRET data are consistent with a movement of TM1a as shown in Fig. 3 (see also Supplementary Movies 1 and 2) and illuminate the function-related dynamic elements in these putative rearrangements. Importantly, as can be seen in Fig. 3 and Supplementary Movie 1, an outward movement of TM1a is essential to create space for leucine to be released to the cytoplasm.

To investigate further how the interaction network at the intracellular end of LeuT contributes to the inward-open conformation, we performed smFRET experiments on H7C/R86C-labelled LeuT constructs in the background of the disruptive mutations R5A or Y268A[32]. As anticipated, we found lower-FRET states for both mutant constructs in the absence of Na^+ (Fig. 4). In both cases, the absolute values of the low-FRET states (~0.43 and ~0.44, respectively) were significantly lower than observed for the wild-type background (~0.51; Supplementary Table 3). These observations indicate that the low-FRET state visited in the wild-type background in the absence of Na^+ might represent a time-averaged population of low-FRET configurations that change in the context of the R5A and Y268A mutations.

Both mutations also affected the FRET distributions observed for extracellularly labelled LeuT (K239C/H480C), indicating that the 'inward opening' effects of these mutations are coordinated with 'outward closing'. We also observed allosteric effects in response to the mutation of Arg 30, which lines the S2 site[10] and participates in the formation of cation-π interactions within a proposed extracellular 'gating region'[9]. In the R30A mutant, H7C/R86C-labelled LeuT adopted a high-FRET configuration in the absence of Na^+ (~0.70), whereas the distance between extracellular pairs (K239C/H480C) was unchanged (Fig. 4 and Supplementary Table 3). These data, corroborated by evidence from the H7C/T515C construct (Supplementary Fig. 3), show that mutations in putative intracellular and extracellular gate regions lead to long-range effects on the conformation of LeuT. However, that the R30A mutation affected the conformation of the intracellular network, while leaving the extracellular probes largely

unchanged, indicates that the transmission of signal throughout the molecule involves a cascade of flexible interactions and local conformations rather than a single rigid body rearrangement[10,32,39].

Also consistent with an allosterically mediated modulation of the interaction network in the intracellular side, the TCA inhibitor clomipramine (CMI) stabilized a high-FRET state (~0.69) in wild-type H7C/R86C-labelled LeuT (Fig. 4). This FRET value, which is distinct from that observed in the absence of CMI (~0.75), was unchanged in the presence of Na^+ (Supplementary Table 3), consistent with the molecular dynamics simulations of LeuT (>100 ns trajectory) with either CMI or OG in the S2 site (and leucine in the S1 site)[15]. These experiments showed that the intracellular network adopted similar and slightly more open configurations when CMI or OG was present in the S2 site, around 30 Å away from residue 7 at the intracellular end of TM1 (Supplementary Fig. 7). On the extracellular side, CMI increased FRET between K239C/H480C-labels (from ~0.49 to ~0.53; Fig. 4), consistent with a modest compaction of this region of LeuT when inhibitor was bound.

To investigate directly whether the conformational changes associated with intracellular gating could be tracked in individual LeuT molecules, we carried out smFRET experiments under conditions that supported extended imaging. First, we reduced the laser illumination intensity to minimize the photobleaching that had previously limited the observation window (~3 s). Second, we increased the exposure time fourfold to 160 ms to maintain signal-to-noise ratios adequate to detect FRET changes at reduced laser intensity. Finally, to eliminate the spontaneous dissociation of LeuT from the image plane that resulted from the relatively low-affinity His–NTA interaction ($k_{off} > 0.25\ min^{-1}$), we introduced a 15-amino-acid C-terminal biotinylation domain[40] into the LeuT (H7C/R86C) construct to allow immobilization by a biotin–streptavidin linkage that is much less prone to dissociation ($k_{off} < 0.25\ h^{-1}$; data not shown).

Given the benefit of an extended observation period, we could show that individual LeuT-H7C/R86C molecules undergo multiple transitions between the high- and low-FRET configurations in the absence of Na^+ (Fig. 5a), consistent with the direct detection of isomerization of the intracellular network. With the reduced illumination intensity, the low-FRET state showed short-lived photophysical 'blinking' events that were probably masked under intense illumination by rapid photoresurrection[36] (see Supplementary Discussion). Taking this into consideration, we could estimate the average dwell time in high- ($\tau \approx 18$ s) and low- ($\tau \approx 25$ s) FRET states, indicating that a full opening–closing cycle required ~60 s. As anticipated from the results of shorter experiments, the high-FRET state was highly stabilized in the presence of high Na^+ concentrations (>76 s, limited by photobleaching; Fig. 5b, c).

We could also assess the unique behaviour of R5A and Y268A LeuT mutants in greater detail under long time-scale imaging conditions. In the absence of Na^+, LeuT-Y268A mainly showed a single, broadened low-FRET state (Fig. 5e). Transitions to higher-FRET states were rare, both with and without substrates. However, consistent with Na^+ binding and partial/incomplete gate closure, the lower-FRET state value increased in the presence of saturating Na^+ and Leu (Fig. 5f, g). In light of the markedly impaired transport activity of LeuT-Y268A (Supplementary Fig. 8), these data point towards a potential correlation between the ability to achieve a properly closed intracellular interaction network and the efficiency of transport. They also support the previous suggestion that the Y335A dopamine transporter (homologous to LeuT Y268A) has low transport activity because it adopts an inward-open conformation[32]. Note that in this mutant, zinc, which is thought to help the transporter reach an outward-facing conformation, markedly enhances transport[32], presumably by facilitating inward closure.

LeuT-R5A showed transient, leucine-dependent isomerization to high-FRET configurations for the 7/86 pair (~0.77), consistent with an inward-closed conformation (compare Fig. 5i, k) and with the finding that its transport activity is much less impaired than that of Y268A (Supplementary Fig. 8). As for LeuT-Y268A, Na^+ alone only shifted the low-FRET state value up slightly. With both substrates present, the lower-FRET state dwell time was similar to that of the wild-type background ($\tau \approx 28$ s), whereas the lifetime of the high-FRET state was substantially reduced compared to the wild-type background ($\tau \approx 8$ s versus $\tau \approx 18$ s, respectively).

In summary, our molecular dynamics and smFRET data indicate that a movement of TM1a is associated with intracellular gating in LeuT. This movement is regulated by substrate and inhibitor binding, by mutations of the intracellular network that stabilizes an inward-closed state, and by mutations of the S2 site, reflecting the allosteric nature of the transport mechanism. Whereas FRET-based single-molecule studies using confocal imaging have provided evidence suggestive of ligand-dependent conformational dynamics in the H^+-coupled sugar transporter lactose permease[41,42], we have obtained minutes-long time-scale FRET trajectories that have directly revealed the relatively slow conformational switching events in LeuT, which would be difficult or impossible to observe using other methods. The extension of imaging times beyond the limit of freely-diffusing molecules using the total internal reflection (TIR) approach, in combination with the surface-immobilization and triplet state quenching strategies, provide a powerful new way to explore the structural and kinetic features of Na^+:substrate symport by LeuT. Extension of these single-molecule imaging approaches to other membrane proteins, as well as to LeuT reconstituted into proteoliposomes in which we can control the Na^+ gradient, will provide further mechanistic details on how the energy stored in ion gradients can be used to drive uphill substrate accumulation by secondary active transporters.

METHODS SUMMARY

LeuT mutants were expressed in *Escherichia coli*, purified, and labelled on targeted engineered cysteines with Cy3 and Cy5 maleimide. We determined the functional properties of the labelled constructs by measuring leucine binding using a scintillation proximity assay, and measured alanine transport after reconstitution of the protein into proteoliposomes. We studied the fluorescence properties of labelled proteins to establish specific and efficient labelling and to confirm that the observed FRET changes probably arise from inter-dye distance rather than photophysical phenomena. We created various constructs, each with two cysteine residues strategically placed for labelling. Purified, labelled protein was immobilized onto a passivated-glass surface with a streptavidin–biotin linkage. We acquired fluorescence data using a prism-based TIR microscope. We calculated FRET efficiency and analysed fluorescence and FRET traces using automated analysis software developed for this application. We analysed the single-molecule traces for LeuT in the presence and absence of the substrates Na^+ and Leu, on addition of the transport inhibitors clomipramine and octylglucoside, and in response to mutations of the extracellular vestibule and the network of intracellular residues that is proposed to stabilize the inward closed state. We carried out molecular dynamics simulations of the protein immersed in an explicit membrane and solvated with water molecules, ions and ligands, and ran long equilibrations (>500 ns) to assess conformational changes.

Full Methods and any associated references are available in the online version of the paper at www.nature.com/nature.

Received 27 November 2009; accepted 23 March 2010.

1. Amara, S. G. & Sonders, M. S. Neurotransmitter transporters as molecular targets for addictive drugs. *Drug Alcohol Depend.* **51**, 87–96 (1998).
2. Rudnick, G. *Mechanisms of Biogenic Amine Neurotransmitter Transporters* 2nd edn (Humana, Totowa, New Jersey, 2002).
3. Sonders, M. S., Quick, M. & Javitch, J. A. How did the neurotransmitter cross the bilayer? A closer view. *Curr. Opin. Neurobiol.* **15**, 296–304 (2005).
4. Gu, H., Wall, S. C. & Rudnick, G. Stable expression of biogenic amine transporters reveals differences in inhibitor sensitivity, kinetics, and ion dependence. *J. Biol. Chem.* **269**, 7124–7130 (1994).
5. Torres, G. E., Gainetdinov, R. R. & Caron, M. G. Plasma membrane monoamine transporters: structure, regulation and function. *Nature Rev. Neurosci.* **4**, 13–25 (2003).
6. Krause, S. & Schwarz, W. Identification and selective inhibition of the channel mode of the neuronal GABA transporter 1. *Mol. Pharmacol.* **68**, 1728–1735 (2005).
7. Iversen, L. Neurotransmitter transporters and their impact on the development of psychopharmacology. *Br. J. Pharmacol.* **147** (suppl. 1), S82–S88 (2006).
8. Beuming, T., Shi, L., Javitch, J. A. & Weinstein, H. A comprehensive structure-based alignment of prokaryotic and eukaryotic neurotransmitter/Na^+

symporters (NSS) aids in the use of the LeuT structure to probe NSS structure and function. *Mol. Pharmacol.* **70,** 1630–1642 (2006).
9. Yamashita, A. *et al.* Crystal structure of a bacterial homologue of Na^+/Cl- dependent neurotransmitter transporters. *Nature* **437,** 215–223 (2005).
10. Shi, L. *et al.* The mechanism of a neurotransmitter:sodium symporter—inward release of Na^+ and substrate is triggered by substrate in a second binding site. *Mol. Cell* **30,** 667–677 (2008).
11. Zhou, Z. *et al.* LeuT-desipramine structure reveals how antidepressants block neurotransmitter reuptake. *Science* **317,** 1390–1393 (2007).
12. Singh, S. K., Yamashita, A. & Gouaux, E. Antidepressant binding site in a bacterial homologue of neurotransmitter transporters. *Nature* **448,** 952–956 (2007).
13. Zhou, Z. *et al.* Antidepressant specificity of serotonin transporter suggested by three LeuT-SSRI structures. *Nature Struct. Mol. Biol.* **16,** 652–657 (2009).
14. Singh, S. K., Piscitelli, C. L., Yamashita, A. & Gouaux, E. A competitive inhibitor traps LeuT in an open-to-out conformation. *Science* **322,** 1655–1661 (2008).
15. Quick, M. *et al.* Binding of an octylglucoside detergent molecule in the second substrate (S2) site of LeuT establishes an inhibitor-bound conformation. *Proc. Natl Acad. Sci. USA* **106,** 5563–5568 (2009).
16. Blanchard, S. C. Single-molecule observations of ribosome function. *Curr. Opin. Struct. Biol.* **19,** 103–109 (2009).
17. Kinosita, K. Jr, Yasuda, R. & Noji, H. F1-ATPase: a highly efficient rotary ATP machine. *Essays Biochem.* **35,** 3–18 (2000).
18. Vale, R. D. Myosin V motor proteins: marching stepwise towards a mechanism. *J. Cell Biol.* **163,** 445–450 (2003).
19. Peterman, E. J., Sosa, H. & Moerner, W. E. Single-molecule fluorescence spectroscopy and microscopy of biomolecular motors. *Annu. Rev. Phys. Chem.* **55,** 79–96 (2004).
20. Ishii, Y., Nishiyama, M. & Yanagida, T. Mechano-chemical coupling of molecular motors revealed by single molecule measurements. *Curr. Protein Pept. Sci.* **5,** 81–87 (2004).
21. Zhuang, X. Single-molecule RNA science. *Annu. Rev. Biophys. Biomol. Struct.* **34,** 399–414 (2005).
22. Cornish, P. V. & Ha, T. A survey of single-molecule techniques in chemical biology. *ACS Chem. Biol.* **2,** 53–61 (2007).
23. Park, H., Toprak, E. & Selvin, P. R. Single-molecule fluorescence to study molecular motors. *Q. Rev. Biophys.* **40,** 87–111 (2007).
24. Ha, T. Need for speed: mechanical regulation of a replicative helicase. *Cell* **129,** 1249–1250 (2007).
25. Schuler, B. & Eaton, W. A. Protein folding studied by single-molecule FRET. *Curr. Opin. Struct. Biol.* **18,** 16–26 (2008).
26. Herbert, K. M., Greenleaf, W. J. & Block, S. M. Single-molecule studies of RNA polymerase: motoring along. *Annu. Rev. Biochem.* **77,** 149–176 (2008).
27. Wen, J. D. *et al.* Following translation by single ribosomes one codon at a time. *Nature* **452,** 598–603 (2008).
28. Pyle, A. M. Translocation and unwinding mechanisms of RNA and DNA helicases. *Annu Rev Biophys* **37,** 317–336 (2008).
29. Noskov, S. Y. & Roux, B. Control of ion selectivity in LeuT: two Na^+ binding sites with two different mechanisms. *J. Mol. Biol.* **377,** 804–818 (2008).
30. Celik, L., Schiott, B. & Tajkhorshid, E. Substrate binding and formation of an occluded state in the leucine transporter. *Biophys. J.* **94,** 1600–1612 (2008).
31. Jorgensen, A. M., Tagmose, L., Bogeso, K. P. & Peters, G. H. Molecular dynamics simulations of Na^+/Cl^--dependent neurotransmitter transporters in a membrane-aqueous system. *ChemMedChem* **2,** 827–840 (2007).
32. Kniazeff, J. *et al.* An intracellular interaction network regulates conformational transitions in the dopamine transporter. *J. Biol. Chem.* **283,** 17691–17701 (2008).
33. Caplan, D. A., Subbotina, J. O. & Noskov, S. Y. Molecular mechanism of ion-ion and ion-substrate coupling in the Na^+-dependent leucine transporter LeuT. *Biophys. J.* **95,** 4613–4621 (2008).
34. Munro, J. B., Altman, R. B., O'Connor, N. & Blanchard, S. C. Identification of two distinct hybrid state intermediates on the ribosome. *Mol. Cell* **25,** 505–517 (2007).
35. Roy, R., Hohng, S. & Ha, T. A practical guide to single-molecule FRET. *Nature Methods* **5,** 507–516 (2008).
36. Dave, R., Terry, D. S., Munro, J. B. & Blanchard, S. C. Mitigating unwanted photophysical processes for improved single-molecule fluorescence imaging. *Biophys. J.* **96,** 2371–2381 (2009).
37. Bennett, E. R., Su, H. & Kanner, B. I. Mutation of arginine 44 of GAT-1, a (Na^+ + Cl^-)-coupled gamma-aminobutyric acid transporter from rat brain, impairs net flux but not exchange. *J. Biol. Chem.* **275,** 34106–34113 (2000).
38. Shaffer, P. L., Goehring, A., Shankaranarayanan, A. & Gouaux, E. Structure and mechanism of a Na^+-independent amino acid transporter. *Science* **325,** 1010–1014 (2009).
39. Lockless, S. W. & Ranganathan, R. Evolutionarily conserved pathways of energetic connectivity in protein families. *Science* **286,** 295–299 (1999).
40. Beckett, D., Kovaleva, E. & Schatz, P. J. A minimal peptide substrate in biotin holoenzyme synthetase-catalyzed biotinylation. *Protein Sci.* **8,** 921–929 (1999).
41. Majumdar, D. S. *et al.* Single-molecule FRET reveals sugar-induced conformational dynamics in LacY. *Proc. Natl Acad. Sci. USA* **104,** 12640–12645 (2007).
42. Nie, Y., Sabetfard, F. E. & Kaback, H. R. The Cys154→Gly mutation in LacY causes constitutive opening of the hydrophilic periplasmic pathway. *J. Mol. Biol.* **379,** 695–703 (2008).

Supplementary Information is linked to the online version of the paper at www.nature.com/nature.

Acknowledgements We thank R. Altman for assistance with reagents for single-molecule experiments; F. Carvalho for the preparation of membranes; J. Munro for help measuring anisotropy; R. Dave for preliminary photobleaching optimization studies; and M. Quick for helpful discussion and comments on the manuscript. Molecular graphic figures and movies were prepared with PyMOL (DeLano Scientific; http://www.pymol.org). Computations were performed on Ranger at the Texas Advanced Computing Center (TG-MCB090022) and the David A. Cofrin computational infrastructure of the Institute for Computational Biomedicine at Weill Cornell Medical College. This work was supported in part by National Institutes of Health Grants DA17293 and DA022413 (J.A.J.), DA12408 (H.W.), and DA023694 (L.S.). D.S.T. is supported by the Tri-Institutional Training Program in Computational Biology and Medicine.

Author Contributions Y.Z. expressed, purified, labelled and functionally characterized the LeuT mutants. Y.Z. and D.T. designed, carried out, and analysed the single-molecule experiments. L.S. and H.W. designed and analysed the computational studies, which were carried out by L.S., S.C.B. and J.A.J. helped to design the biochemical and single-molecule experiments and, with L.S. and H.W., helped to interpret the data. All the authors contributed to writing and editing the manuscript.

Author Information Reprints and permissions information is available at www.nature.com/reprints. The authors declare no competing financial interests. Readers are welcome to comment on the online version of this article at www.nature.com/nature. Correspondence and requests for materials should be addressed to J.A.J. (jaj2@columbia.edu) or S.C.B. (scb2005@med.cornell.edu).

METHODS

Protein expression and purification. Wild-type and mutant LeuT were produced in *E. coli* C41(DE3) harbouring pQO18 or pETO18G and purified by immobilized metal (Ni^{2+}) affinity chromatography using a Ni^{2+} Sepharose 6 FastFlow column (GE Healthcare). We prepared membrane vesicles and purified LeuT variants as described[43]. For Cy3 or Cy5 labelled protein, after the protein was immobilized on the Ni^{2+} Sepharose 6 FastFlow resin, the resin was washed with 5 column volumes of Buffer A: 50mM Tris/Mes (pH 7.5), 150 mM NaCl, 1 mM TCEP, 20% Glycerol, 0.05% w/v (1 mM) *n*-dodecyl-β-d-maltopyranoside (DDM), and 50 mM imidazole. We then washed the resin with 5 column volumes of labelling buffer: 50 mM Mes (pH 6.0), 400 mM NaCl, 200 μM lysine, 50 μM TCEP, 1 mM DDM. After the resin was resuspended in labelling buffer, 200 μM Cy3 and 200 μM Cy5 maleimide (GE Healthcare) were added to the solution and reacted for 1 h at 4 °C while rotating the column. To remove free Cy3 and Cy5, we reloaded the resin into the column and washed it with 5 column volumes of buffer A. The protein was eluted in Buffer A with 300 mM imidazole and purified with HPLC-mediated size-exclusion chromatography (Shodex Protein-KW803 column) in Buffer B: 50 mM Tris/Mes (pH 7.5), 150 mM NaCl, 1 mM TCEP, 1 mM DDM.

We estimated the extent of the labelling from absorption spectra of labelled protein by measuring peak maxima at 552 nm and 650 nm for Cy3 and Cy5, respectively, using a Hitachi model 24 UV-VIS scanning spectrophotometer. We determined protein concentration using the amido black method[44]. Under the same conditions, control labelling experiments of wild-type LeuT, which is devoid of cysteine, resulted in no significant incorporation of Cy3 or Cy5 dyes. Final samples were flash frozen and stored at –80 °C before use.

We performed site-directed replacement of single residues by cysteine using the Stratagene Quikchange mutagenesis kit. To confirm the fidelity of all plasmids, we used DNA sequencing (Agencourt Bioscience Corporation).

Creation of biotin acceptor peptide tagged pETO18G. We removed an existing BamHI restriction site from the pETO18G plasmid by silent modification (ACG to ACA) at amino acid position 135. We used the Stratagene Quikchange mutagenesis kit to mutate the stop codon (TGA) to GGA. We then introduced the biotin Acceptor Peptide (AP) sequence GLNDIFEAQKIEWHE[40] and a stop codon (TGA) using XhoI and BamHI restriction sites and primers AP-F (TCGAGGGGCTTAATGATATCTTTGAAGCTCAGAAAATTGAATGGCATG AGTGAG) and AP-R (GATCCTCACTCATGCCATTCAATTTTCTGAGCTT CAAAGATATCATTAAGCCCC).

Biotinylated protein expression. We co-transformed pBirAcm (AVIDITY LLC) and AP-tagged pETO18G into *E. coli* C41 (DE3). At $OD_{600} = 0.5$, we added 10 μM D-biotin, induced expression with 0.3 mM IPTG, and grew cells overnight at 20 °C.

Scintillation proximity-based binding studies. We bound ^{3}H-leucine (140 Ci mmol^{-1}; Moravek) to purified LeuT-variants using the scintillation proximity assay (SPA) as described[10,43] with 25 ng of purified protein per assay in buffer composed of 50 mM Tris/Mes (pH 8.0), 100 mM NaCl, 1 mM TCEP, 20% glycerol and 1 mM DDM .

Transport and binding in proteoliposomes. We prepared liposomes using *E. coli* polar lipid extract and phosphatidylcholine (Avanti) at a 3:1 (w/w) ratio, as described[10]. We reconstituted purified LeuT variants at a 1:150 (w/w) ratio in preformed, Triton X-100-destabilized liposomes. We measured the accumulation of ^{3}H-Ala (49.4 Ci mmol^{-1}; Moravek) at 23 °C in assay buffer comprising 50 mM Tris/Mes (pH 8.5) and 50 mM NaCl. We assessed binding of ^{3}H-Ala to LeuT proteoliposomes by dissipating the electrochemical NaCl gradient with 25 μg ml^{-1} gramicidin for 5 min before the start of the reaction. Uptake reactions were stopped by quenching the samples with ice-cold assay buffer followed by rapid filtration through GF/F filters (Advantec MFS).

Steady-state fluorescence anisotropy measurements. We carried out steady-state anisotropy measurements of Cy3-labelled LeuT (10 nM) using a PTI spectrofluorometer with excitation and emission wavelengths of 532 nm and 560 nm, respectively.

Calculation of distances from FRET efficiencies. We estimated distances between Cy3 and Cy5 in specific FRET states using the following equation:

$$R = R_0 \sqrt[6]{\frac{1-E}{E,}}$$

where R_0 is the distance at which 50% energy transfer is observed. The experimentally determined R_0 of 58.4 Å was estimated according to the equation[45]:

$$R_0 = 0.221 \sqrt[6]{\Phi_D \kappa^2 \eta^{-4} J(\lambda)}$$

where the refractive index of the experimental solution (η) was estimated to be 1.4 and the orientation factor, κ^2, was assumed to be 2/3 given isotropic rotation on the millisecond timescale . The spectral overlap integral $J(\lambda) = 8.5 \times 10^{-13}$ M^{-1} cm^3 was calculated using the normalized fluorescence emission spectrum of Cy3-7C-LeuT and the absorption spectrum of Cy5-7C-LeuT collected using bulk fluorescence instrumentation (Photon Technologies). The Cy3 and Cy5 extinction coefficients used in calculation[46] were: $\varepsilon_{550(Cy3)} = 150{,}000$ M^{-1} cm^{-1} and $\varepsilon_{650(Cy5)} = 250{,}000$ M^{-1} cm^{-1}.

The donor quantum yield of Cy3-7C-LeuT ($\Phi_{Cy3} = 0.23$) was estimated using the comparative method[47] using Rhodamine 101 in ethanol as a standard ($\Phi_{R101} \approx 1.0$)[48]. We collected the fluorescence emission spectra of both dyes with excitation at 520 nm using constant illumination intensity and slit widths. We calculated the Cy3 quantum yield as follows:

$$\Phi_{Cy3} = \Phi_{Rh101} \times \left(\frac{F_{Cy3}}{F_{R101}}\right) \times \left(\frac{A_{R101}}{A_{Cy3}}\right) \times \left(\frac{\eta_{Cy3}}{\eta_{R101}}\right)^2$$

where F_{Cy3} and F_{R101} are the integrated fluorescence emission spectra; A_{Cy3} and A_{R101} are the absorbances; and $\eta_{Cy3} = 1.4$ and $\eta_{R101} = 1.36$ are the refractive indices of the solutions used for Cy3-LeuT (the buffer used for single-molecule experiments) and Rhodamine 101 (ethanol), respectively.

Single-molecule FRET experiments. We acquired fluorescence data using a prism-based TIR microscope, as described[34]. All experiments were performed in buffer containing 50 mM Tris/MES (pH 7.5), 10% glycerol, 0.02% w/v DDM, 5 mM 2-mercaptoethanol and 200 mM salt (KCl or NaCl, as specified). We used an oxygen scavenging environment (1 unit per μl glucose oxidase, 8 units per μl catalase, 0.1% v/v glucose) containing 1 mM cyclooctatetraene in all experiments to minimize photobleaching[36].

We incubated microfluidic imaging chambers passivated with a mixture of PEG and biotin-PEG[49] with 0.8 μM streptavidin (Invitrogen), followed by 20 nM biotin-NTA (Biotium) charged with $NiCl_2$. Cy3/Cy5-labelled His_{10}-LeuT molecules (2 nM) were surface-immobilized to surface-bound Ni^{2+}. We observed no significant surface immobilization, measured as described below, in the absence of biotin-NTA (Supplementary Fig. 2).

Cy3 fluorophores were excited by the evanescent wave generated by TIR of a single-frequency light source (Ventus 532 nm, Laser Quanta). Photons emitted from Cy3 and Cy5 were collected using a 1.2 NA 60× water-immersion objective (Nikon), and optical treatments were used to spatially separate Cy3 and Cy5 frequencies onto a cooled, back-thinned CCD (Cascade 128, Photometrics). We acquired fluorescence data using MetaMorph software (Universal Imaging Corporation). We corrected spectral bleed-through of Cy3 intensity on the acceptor channel by subtracting 7.5% of donor signal from the acceptor. FRET traces were calculated as: $\text{FRET} = I_{Cy5}/(I_{Cy3} + I_{Cy5})$, where I_{Cy3} and I_{Cy5} are the instantaneous Cy3 and Cy5 fluorescence intensities, respectively. Using an established procedure[35], we estimated the ratio of donor and acceptor quantum yields and detection efficiencies (γ) to be close to 1; therefore, no correction was applied.

Analysis of smFRET traces. We analysed fluorescence and FRET traces using automated analysis software (D.T., M.B. Feldman, R.B. Altman and S.C.B., manuscript in preparation), in which traces were selected using algorithms implemented in MATLAB (MathWorks). Properties were calculated for each trace, and selected for further analysis if they met the following specific criteria: a single photobleaching event, at least 8:1 signal-to-background noise ratio (SNR), <4 donor fluorophore blinking events, a donor-to-acceptor Pearson's correlation coefficient <0.5, and a lifetime of at least 15 frames showing FRET ≥0.15. We detected photobleaching events in each trace as a significant (≥3 standard deviations of background noise) drop in the median-filtered (window size of 9 frames) total fluorescence intensity ($I_{Total} = I_{Cy3} + I_{Cy5}$) without a return to the previous average level. Events in which fluorescence intensity did return were marked as blinking events. Signal-to-noise ratios are calculated as total intensity relative to the standard deviation of background noise: $I_{Total}/[\text{stdev}(I_{Cy3}) + \text{stdev}(I_{Cy5})]$. We excluded data points corresponding to donor fluorophore dark states from calculation of the correlation coefficient.

To simplify the presentation of FRET histograms, we removed zero-FRET states following idealization of the data to a two-state model ($E = 0.1 \pm 0.1$ and $E = 0.4 \pm 0.1$) using a segmental *k*-means algorithm[50]. Error bars in FRET histograms represent the standard deviation of 100 bootstrap samples of each set of FRET traces examined.

We estimated kinetic parameters for biotinylated H7C-R86C-LeuT samples by manually selecting traces showing at least one transition between clearly distinct states with anti-correlated changes in donor and acceptor fluorescence intensity in each transition. The data were then idealized using a three-state model ($E = 0 \pm 0.1$, $E = 0.49 \pm 0.09$, and $E = 0.75 \pm 0.07$) with FRET parameters estimated by fitting smFRET histograms obtained in the absence of Na^+ to Gaussian functions. Initial rates were set to 0.05 s^{-1}, as estimated from visual inspection of FRET traces. We estimated average dwell times in each FRET state using a maximum likelihood algorithm[51].

Molecular dynamics. We carried out simulations on the system prepared as described[10]. Briefly, it consisted of more than 77,000 atoms, including the explicit membrane model, solvating water molecules, and the various ions and ligands. Each of the simulations was started from the end of the previously described SMD trajectory in which the ligand in the S1 site was pulled towards the intracellular side and had reached 8–10 Å below the S1 binding site[10]. The molecular dynamics simulations were carried out with the NAMD program under constant temperature (310 K) and constant pressure (1 atm) (NPT) conditions. The equilibrations were long (150 ns), to achieve a suitable relaxation of the system. We carried out two independent runs for the system, for consistency and convergence check. The results of one run are compared in Fig. 3 with those of a control run[10] starting from the crystal structure (PDB accession 2A65, in an inward-closed state), to illustrate the level of stability and fluctuation of the system under the simulation conditions.

43. Quick, M. & Javitch, J. A. Monitoring the function of membrane transport proteins in detergent-solubilized form. *Proc. Natl Acad. Sci. USA* **104,** 3603–3608 (2007).
44. Schaffner, W. & Weissmann, C. A rapid, sensitive, and specific method for the determination of protein in dilute solution. *Anal. Biochem.* **56,** 502–514 (1973).
45. Lakowicz, J. R. *Principles of Fluorescence Spectroscopy* 3rd edn (Springer, 2006).
46. Mujumdar, R. B. *et al.* Cyanine dye labeling reagents: sulfoindocyanine succinimidyl esters. *Bioconjug. Chem.* **4,** 105–111 (1993).
47. Williams, A., Winfield, A. S. & Miller, N. J. Relative fluorescence quantum yields using a computer-controlled luminescence spectrometer. *Analyst (Lond.)* **108,** 1067–1071 (1983).
48. Karstens, T. & Kobs, K. Rhodamine B and rhodamine 101 as reference substances for fluorescence quantum yield measurements. *J. Phys. Chem.* **84,** 1871–1872 (1980).
49. Blanchard, S. C. *et al.* tRNA dynamics on the ribosome during translation. *Proc. Natl Acad. Sci. USA* **101,** 12893–12898 (2004).
50. Qin, F. Restoration of single-channel currents using the segmental k-means method based on hidden Markov modeling. *Biophys. J.* **86,** 1488–1501 (2004).
51. Qin, F., Auerbach, A. & Sachs, F. Estimating single-channel kinetic parameters from idealized patch-clamp data containing missed events. *Biophys. J.* **70,** 264–280 (1996).

SUPPLEMENTARY INFORMATION

Supplementary Discussion:

Photophysical transitions to zero-FRET in 160 ms FRET trajectories.

The smFRET traces obtained during low-power illumination of dye-labeled H7C/R86C-LeuT undergo frequent, transient zero-FRET state excursions, often referred to as photophysical "blinking" events (**Fig. 5**). Such events, frequently observed during single-molecule fluorescence imaging, typically result from the intersystem crossing of the acceptor fluorophore (Cy5) to non-fluorescent dark states[1]. Blinking events are characterized by having a strong laser power dependence on the observed rates entering and exiting dark states. Although the triplet state quenching strategies employed greatly reduce the lifetimes of these states, under low-power illumination the rate of return to the fluorescing state approaches the imaging timescale (160ms). Consequently, rapid transitions to low and zero FRET states were assigned as Cy5 dark states. In line with the statistical labeling strategy employed for the introduction of fluorophores into LeuT and the environmentally sensitive nature of dye photophysics[1], blinking events of this nature were observed for only ~50% of the labeled molecules, predominantly from the lower-FRET (≤0.6) states. Several of the traces shown in Fig. 5 have this blinking behavior, which serves as additional evidence of conformational transitions between structurally distinct LeuT conformations.

Interpretation of changes in FRET efficiency.

Time-dependent fluctuations in FRET efficiency observed in experiments with LeuT labeled at position H7C+R86C and H7C+T515C are interpreted as principally reporting on changes in the distance between donor and acceptor dyes reflecting underlying changes in LeuT structure. For such a FRET-distance relationship to hold, one or both fluorophores must be freely rotating on the timescale of imaging (κ^2=2/3) and fluorophore quantum yield (Supplementary Methods) must remain relatively constant over the imaging period. Both κ^2 and quantum yield impinge on the FRET-distance relationship *via* the parameter R_0.

To test the possibility that the changes in FRET observed do not simply report on changes in quantum yield, fluorescence quantum yields of Cy3 and Cy5 at position 7 and 86 in LeuT were measured under conditions where FRET changes in LeuT are observed (e.g. +/- ligand as shown in (Fig. 2)). Consistent with the notion that quantum yield remains relatively constant under conditions where substantial changes in FRET were observed, changes in

spectral shift were not observed and the fluorescence intensities of Cy3-labeled LeuT in the absence and presence of saturating ligand concentrations (200 mM) and/or Leu (20 μM) were indistinguishable within approximately 10% experimental error (data not shown). Additionally, the measured fluorescence lifetimes of Cy3-7C-LeuT and Cy5-7C-LeuT samples were also independent of ligand concentration (data not shown).

To test whether the observed fluctuations in FRET efficiency result from changes in the extent of randomization of dye orientation during imaging, Cy3 anisotropy was measured at multiple sites of labeling (Supplementary Table 2). The measured anisotropy values (r = ~0.22), while indicative of somewhat restricted or slowed Cy3 motion when the dye is linked to LeuT, is consistent with substantial randomization of orientation on the imaging time scale (40-160ms), particularly given the dye's relatively short fluorescence lifetime (<1.5 ns). Again, no systematic changes in anisotropy were observed in the absence and presence of Na^+ (200 mM) and/or Leu (20 μM).

Although changes in dye quantum yield and/or relative orientation could complicate the FRET-distance relationship interpretation, fluctuations in these parameters are anticipated to occur on the sub-millisecond timescale, substantially more rapid than the timescale of the FRET changes observed (tens of seconds). The likelihood that significant contributions to the measurement result from spurious changes in these parameters is reduced by the number of internally consistent data obtained when examining distinct pairs of labeling sites, ligand-binding and LeuT mutations distal to the site of labeling. Therefore, the evidence supports the interpretation that changes in FRET principally arise from changes in distance between the dyes resulting from changes in LeuT structure.

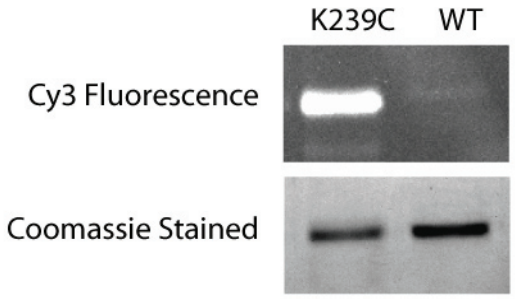

Supplementary Figure 1: Site-specific dye-labeling of LeuT. Wild-type LeuT and a representative Cys substitution mutant (LeuT-K239C) were expressed and purified as described in Supplementary Methods and run on 12% gel. The labeling buffer: 50 mM Mes (pH 6.0), 400 mM NaCl, 200 μM lysine, 50 μM TCEP, 200 μM Cy3-maleimide. LeuT- K239C was efficiently labeled, as shown by high fluorescence (535 nm longpass filter), but not the wild-type sample, which has no native cysteine residues. (Bottom Panel) The same gel stained with Coomassie blue.

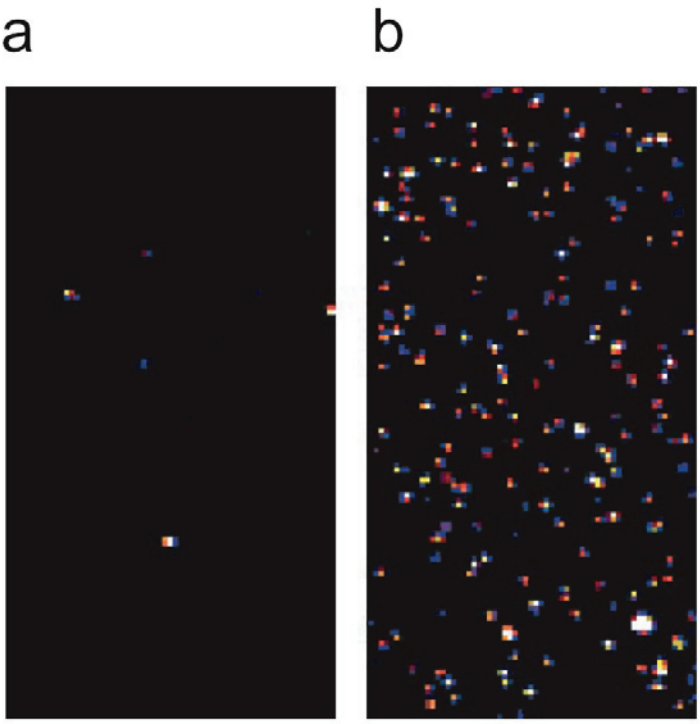

Supplementary Figure 2: Specificity of surface immobilization strategy. Surfaces were incubated with (**a**) streptavidin or (**b**) streptavidin and biotin-NTA as described in Supplementary Methods. Dye-labeled samples were injected and washed after 3 minutes. Without biotin-NTA, few molecules adhered to the surface, whereas many isolated molecules can be seen when surfaces are treated with biotin-NTA.

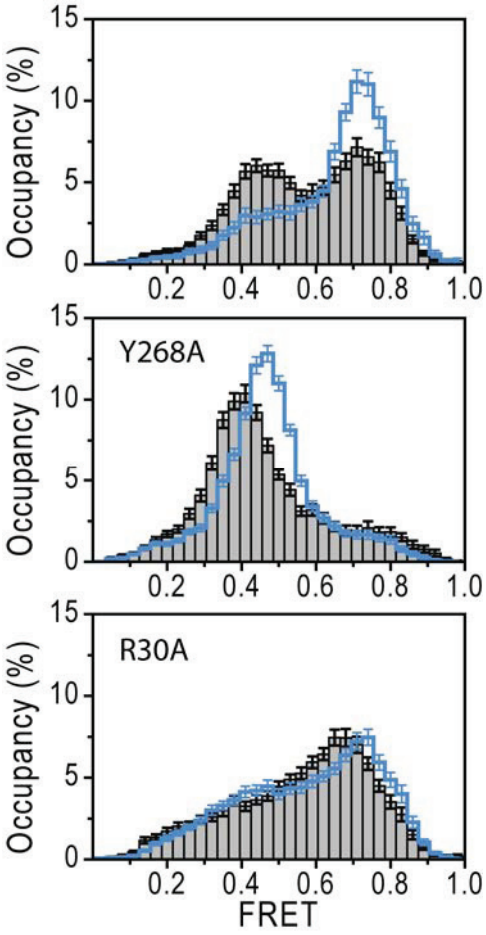

Supplementary Figure 3: smFRET imaging experiments were performed with intracellularly labeled LeuT-H7C-T515C in wild-type, the Y268A "intracellular gate" mutant, and the R30A "extracellular gate" mutant. Experiments were performed in the absence of Na^+ (200 mM KCl) (gray bars) or in its presence (200 mM NaCl) (blue line).

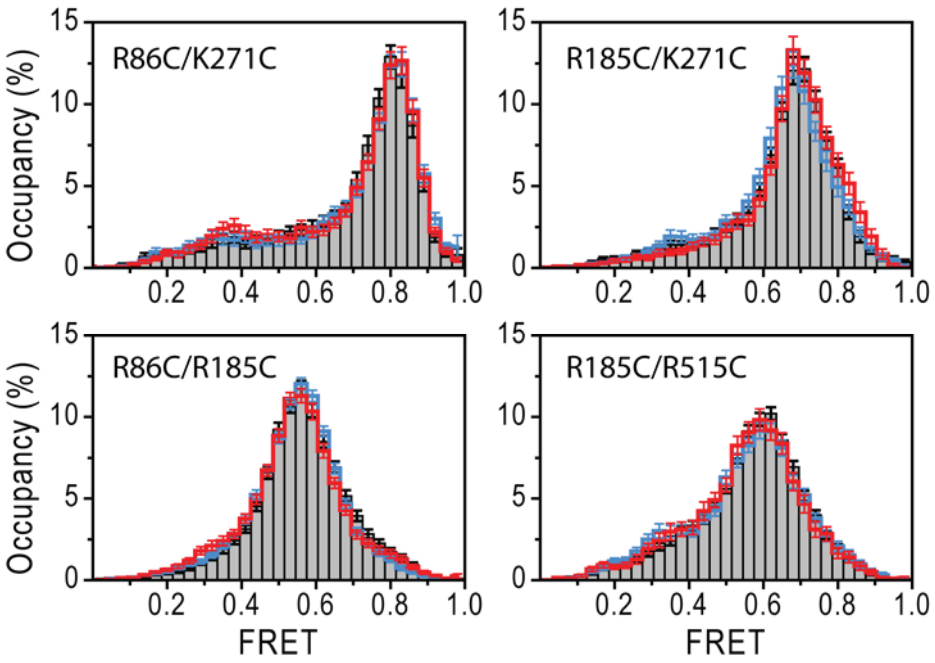

Supplementary Figure 4: smFRET imaging experiments were performed with LeuT labeled at several intracellular sites: R86C+K271C, R185C+K271C, R86C+R185C, R185C+T515C. FRET traces were summed into histograms for experiments performed in the absence of Na+ (gray bars). No significant changes in the FRET distributions were observed in the presence of 200 mM NaCl (blue line), in the absence of Na^+ (gray bars), or in the presence of 200 mM NaCl and 20 μM Leu (red line).

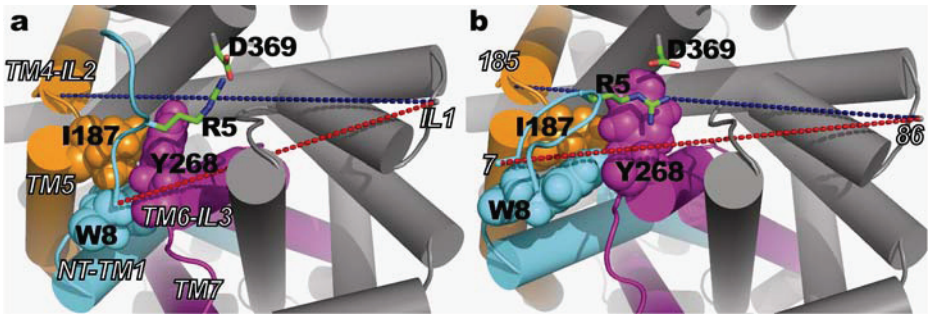

Supplementary Figure 5: Schematic representations of the observed dynamic changes in a structural context. Panels (**a**) and (**b**) show the distances measured with smFRET in the context of the changes in LeuT conformations observed at the end of simulations exploring inward-closed and inward-open states, respectively (see also Figure 3b and Movies). The blue line connecting positions (86-185) and the red line (7-86) identify the monitored distances shown in Fig. 3a. The residues rendered in color form the "intracellular interaction network" centered on Tyr268, which highlights the configurational changes in the triad of interactions among NT-TM1 (cyan), TM4-IL2-TM5 (orange), and TM6-IL3-TM7 (purple) in the two states.

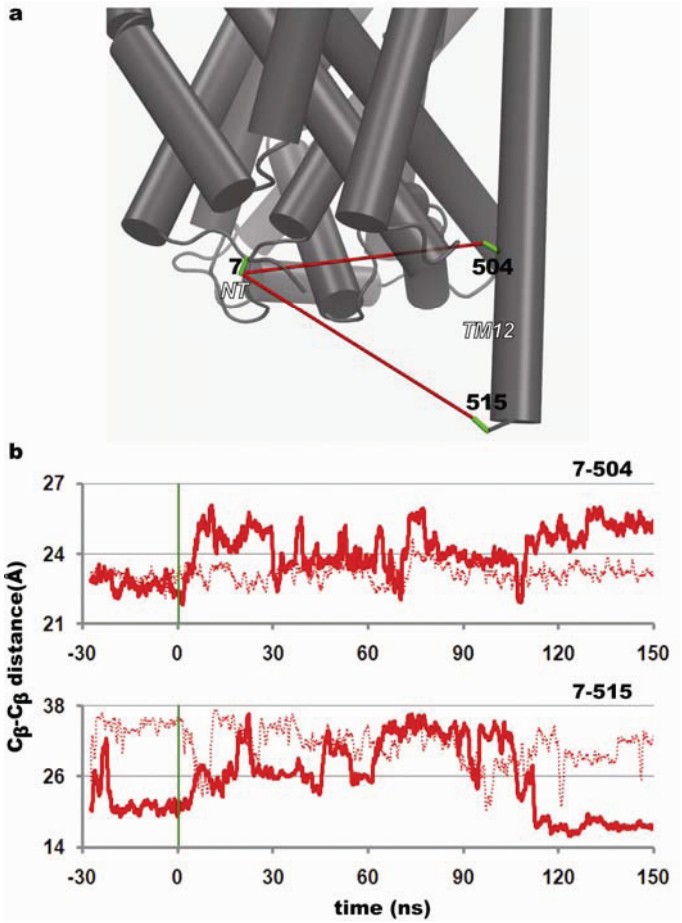

Supplementary Figure 6: Molecular dynamics data for the 7-515 and 7-504 pairs of residues. Since 515 is located at the distal end of TM12, relatively far below the membrane boundary (see Fig. 1a), in the aqueous environment (panel a), the C-terminal segment in which it resides exhibits high flexibility, much greater than that expected in the smFRET experiment where this terminus is anchored and embedded in the surrounding detergent. Thus, the MD data for the 7/515 pair exhibit relatively large fluctuations that exaggerate the actual motions observed experimentally (panel b). However, the relevant motion of TM12 relative to NT-TM1 is reliably described by the distance between 7 and position 504, which is located near the membrane boundary. The 7/504 distance changes during the MD simulation shown in panel b demonstrate a gradual evolution towards a stable increased distance, consistent with the corresponding experimental measurements.

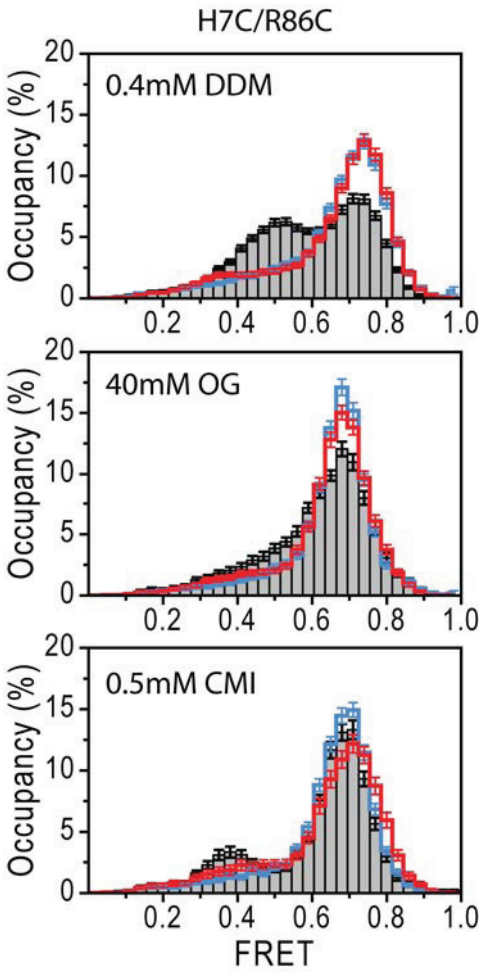

Supplementary Figure 7: Effect of detergents on the intracellular conformation and ligand sensitivity of LeuT. Dye-labeled LeuT-H7C/R86C was imaged in the presence of 0.4 mM DDM or after exchanging with buffer containing n-octyl-β-D-glucoside (OG) or with 0.5 mM CMI in 0.4 mM DDM. Experiments were performed in the absence of Na^+ (black bars), in 200 mM NaCl (blue lines), or in the presence of 200 mM NaCl and 20 μM Leu (red lines).

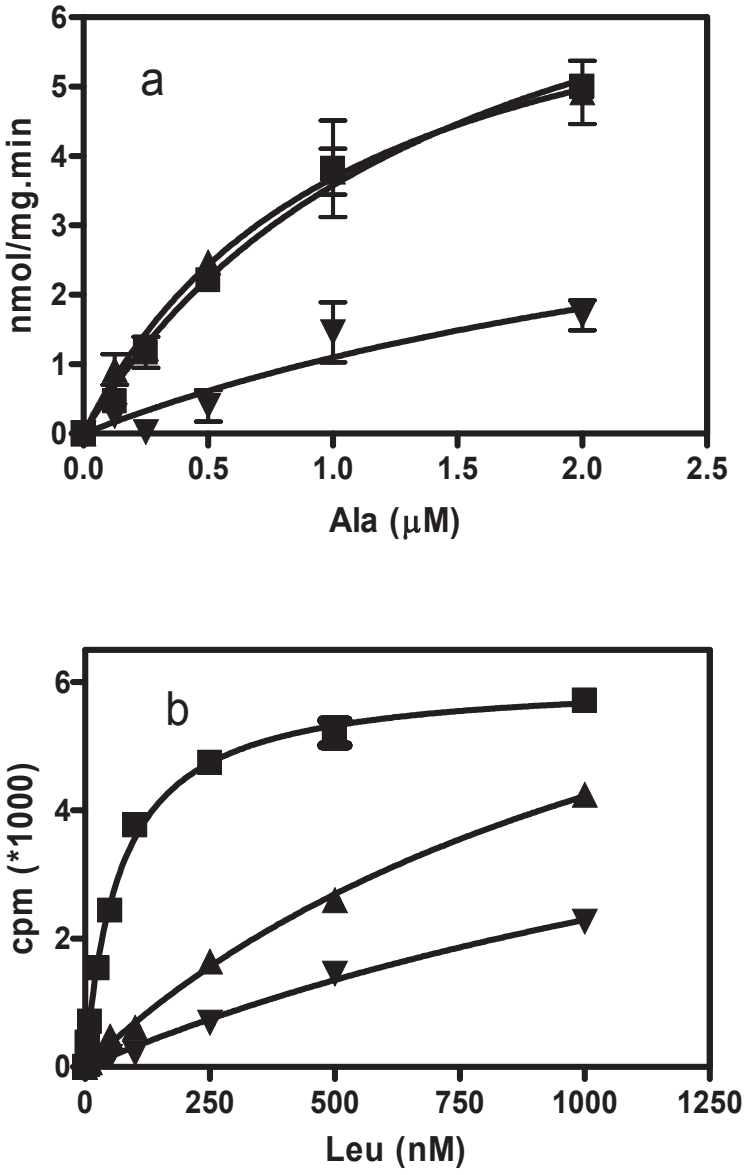

Supplementary Figure 8: Activity of intracellular gate mutants. (**a**) Ala transport and (**b**) Leu binding activities were measured in wild-type (squares ■), R5A (triangles ▲) and Y268A (inverted triangles▼) LeuT. Error bars represent the standard deviation from three independent experiments.

Labeling Position	Buffer A (No Na)	Buffer B (Na)	Buffer C (Na+Leucine)	H_2O
Free dye	0.136	0.157	0.156	0.156
R185C	0.233	0.229	0.239	n.d.
H7C	0.207	0.228	0.205	n.d.
R86C	0.200	0.216	0.218	n.d.
T515C	0.131	0.213	0.201	n.d.
K271C	0.212	0.200	0.224	n.d.

n.d.: No data.

Supplementary Table 1: Bulk dye anisotropy measurements. Fluorescence anisotropy (r) was measured for Cy3 free in solution or chemically attached to several different substituted Cys in LeuT using a bulk fluorimeter (PTI Instruments). Buffer A contained 200 mM KCl, Buffer B contained 200 mM NaCl, and Buffer C contained 200 mM NaCl and 20 μM Leu. Error in measured anisotropy values was ≤2% in all cases (standard deviation of three measurements).

Labeling Positions	Leu binding activity (% of wild-type)	Ala uptake activity (% of wild-type)
H7C/R86C	94±2%	112±2%
H7C/T515C	107±3%	110±12%
R185C/K271C	93±2%	94±4%
R185C/T515C	112±2%	108±4%
R86C/K271C	96±2%	96±20%
R86C/R185C	83±3%	89±4%
K239C/H480C	91±7%	105±2%

Supplement Table 2: Substrate binding and transport activity for double-labeled LeuT. Several double cysteine mutant LeuT samples were labeled with Cy3 and Cy5 (1:1 molar ratio) and purified in detergent. Binding activity was assessed by measuring of ^{3}H-Leu binding to LeuT using a scintillation proximity assay (SPA). Dye-labeled LeuT was reconstituted into liposomes, and transport activity was assessed by measuring the rate of ^{3}H-Ala (1 μM) accumulation in proteoliposomes in 50 mM Tris/Mes (pH 8.5), 50 mM NaCl at room temperature for 10 min. Errors are the standard deviation of three separate experiments.

Labeling Position	Mutation/ Inhibitor	Ligands	Observed FRET	Corrected FRET	Dye-to-Dye Distance (Å)
7+86			0.51	0.59	55
			0.75	0.88	42
		Na	0.77	0.91	40
		Na+Leu	0.77	0.91	40
	R5A		0.43	0.49	59
		Na	0.54	0.62	54
	Y268A		0.44	0.50	58
		Na	0.56	0.65	53
	R30A		0.70	0.82	45
		Na	0.71	0.83	45
		Na+Leu	0.71	0.83	45
	CMI		0.69	0.81	46
		Na	0.69	0.81	46
	OG		0.68	0.80	47
		Na	0.68	0.80	47
239+480			0.49	0.56	56
		Na	0.51	0.59	55
		Na+Leu	0.52	0.60	55
	R5A		0.66	0.77	48
	Y268A		0.67	0.78	47
	R30A		0.49	0.56	56
		Na	0.52	0.60	55
		Na+Leu	0.52	0.60	55
	CMI		0.53	0.61	54
7+515			0.43	0.49	59
			0.73	0.86	43
		Na	0.73	0.86	43
		Na+Leu	0.74	0.87	43
	Y268A		0.40	0.46	60
		Na	0.46	0.53	57
	R30A		0.67	0.78	47
		Na	0.72	0.85	44
86+185			0.58	0.67	52
		Na	0.58	0.67	52
		Na+Leu	0.57	0.66	52
185+515			0.61	0.71	50
		Na	0.61	0.71	50
		Na+Leu	0.61	0.71	50
86+271			0.80	0.95	36
		Na	0.80	0.95	36
		Na+Leu	0.80	0.95	36
185+271			0.70	0.82	45
		Na	0.68	0.80	47
		Na+Leu	0.71	0.83	45

Supplementary Table 3: Estimation of distances from FRET values.

For each dye-labeled sampled under each solution condition, FRET data were summed into histograms (bin size=0.015) and fit to a sum of Gaussian distribution functions. The observed

FRET values are distorted by spectral bleed-through (also referred to as crosstalk) that arises from imperfections in the spectral separation using dichrioic mirrors. As a result, some fraction (α) of Cy3 emission appears as Cy5 intensity and some fraction (β) of Cy5 emission appears as Cy3 intensity. To arrive at estimated distances for each FRET value the following correction for bleed-through was applied to the uncorrected FRET values:

$$E = \frac{E_{obs} - \alpha}{1 - \beta - \alpha},$$

where α=0.075 and β=0.155 were estimated from the fluorescence emission spectra of Cy3 and Cy5 and the transmission spectra of optical components in the light path. Corrected FRET values were then used to calculate an average distance (R) between Cy3 and Cy5 in each experiment (Supplemental Methods). We estimate the upper limit of the error in the distances to be ±5Å.

Supplementary Movies: Conformational changes in the simulated transport mechanism

The two movies show the time evolution of a superposition of the trajectories (~180 ns each) from MD equilibrations of the crystal structure of LeuT (in gray) and an SMD/MD simulation that induces and equilibrates the inward-open structure (in orange). The structure superposition is based on the conserved TMs (1, 3, 6, and 8). The α-helical regions are shown as cylinders. The descending S1 substrate (Leu) is rendered in functional colors. The SMD/MD simulation was started from the configuration with substrates in both the S1 and S2 sites (Methods for details). Movie I presents a side view (parallel to the membrane) with the intracellular portion at the bottom. Movie II presents the same data, viewed from the intracellular side. The evolving differences in structural rearrangements of the gray and orange structures identify the conformational changes in the simulated transport mechanism. These changes agree with and are reflected in the results from the smFRET measurements.

References:

52. Dave, R., Terry, D. S., Munro, J. B., and Blanchard, S. C., Mitigating unwanted photophysical processes for improved single-molecule fluorescence imaging. *Biophys J* 96 (6), 2371-2381 (2009).

There is also a possibility that Willenbring and von Blanckenburg[1] partly miss the mountain-uplift signal on the global carbon cycle because their beryllium record does not extend far enough into the past. Himalayan uplift started some 40 million years ago, but intensified around 20 million years ago. At the same time, the monsoon regime strengthened, with enhanced rainfall on the southern flank of the range[9]. Today, erosion rates in the Himalayan range are controlled by the intensity of the monsoon[10]. So the imprint of this major mountain range on the global erosion rate of the continents might have begun some 10 million years before the oldest beryllium isotopic record. It is possible that the Himalaya have been consuming CO_2 at the present-day rate for 20 million years. If so, they are still influencing the carbon cycle and global climate but this might be undetectable in the beryllium record, which spans too short a period.

Whatever the questions raised by the work of Willenbring and von Blanckenburg[1], their study challenges our understanding of the mechanisms controlling evolution of the Earth system. It will lead to a necessary rethink of the tight links between tectonic activity, physical erosion, chemical weathering and, ultimately, climate change. ■

Yves Goddéris is at the LMTG-Observatoire Midi-Pyrénées, CNRS, Université de Toulouse III, Toulouse F-31400, France.
e-mail: godderis@lmtg.obs-mip.fr

1. Willenbring, J. K. & von Blanckenburg, F. *Nature* **465,** 211–214 (2010).
2. Zachos, J. C., Dickens, G. R. & Zeebe, R. E. *Nature* **451,** 279–283 (2008).
3. Ruddiman, W. F. (ed.) *Tectonic Uplift and Climate Change* (Plenum, 1997).
4. France-Lanord, C. & Derry, L. A. *Nature* **390,** 65–67 (1997).
5. Galy, V. *et al. Nature* **450,** 407–410 (2007).
6. Zhang, P., Molnar, P. & Downs, W. R. *Nature* **410,** 891–897 (2001).
7. Pagani, M., Zachos, J. C., Freeman, K. H., Tipple, B. & Bohaty, S. *Science* **309,** 600–603 (2005).
8. Raymo, M. E. *Geology* **19,** 344–347 (1991).
9. Guo, Z. T. *et al. Nature* **416,** 159–163 (2002).
10. Galy, A. & France-Lanord, C. *Geology* **29,** 23–26 (2001).

BIOPHYSICS

Transporter in the spotlight

Nathan K. Karpowich and Da-Neng Wang

Membrane transporter proteins switch between conformational states to move substrates across membranes. The transition between these states can now be studied using single-molecule experiments.

Biologists who work with membrane transporters — proteins that ferry substrate molecules across membranes — have long been envious of their colleagues who study ion channels. For more than three decades, researchers have been able to observe the dynamic opening and closing of single ion channels in real time using single-channel recording techniques[1]. The ability to watch ion channels 'dance' as they conduct a current allows the functional states of these proteins to be identified, and provides clues about their gating mechanisms. By contrast, bar a few notable exceptions[2,3], secondary membrane transporters can't be studied in this way. But in this issue, Zhao *et al.*[4] (page 188) report the use of a fluorescence technique to visualize several steps in the cycle of a transporter as it translocates a substrate. This is a breakthrough in the field.

Secondary membrane transporters are ubiquitous, dynamic, molecular machines that use electrochemical gradients across membranes to drive the movement of substrates 'uphill' through those membranes — that is, against the prevailing concentration gradient of the substrate[5]. Various research, including several X-ray crystal structures[6,7], has greatly enhanced our understanding of the substrate specificity and translocation pathways in these proteins.

But such spectacular structures can only suggest the motions that are crucial to membrane transport cycles. Two important pieces of information remain missing[8]. The first is the dynamics of the transport cycle: how much time does the transporter stay in a particular state or in transition between states, and how does the protein's conformation change during transition? Single-channel recording cannot answer these questions, because the transport cycles are too slow, and the total transported substrates are often unchanged.

The second area of ignorance is an even greater embarrassment: we don't know how many conformational states exist in the transport cycles of secondary membrane transporters. Ion channels can be trapped in particular states by certain toxins, as can primary transporters by analogues of the nucleotide ATP. But molecular tools for dissecting the individual conformations of secondary transporters are missing. As a result, many of the mechanistic details of these proteins remain unresolved.

Enter Zhao *et al.*[4], who have used a technique known as single-molecule fluorescence resonance energy transfer (smFRET) to study the LeuT transporter. Found in bacteria, LeuT belongs to the neurotransmitter/sodium symporter family of proteins, which couple the uphill uptake of substrates into cells to the downhill transport of sodium ions[9]. The LeuT transporter is a pore that contains two gates: an inner gate that opens to the cell lumen, and an outer gate that opens to the cell's exterior. The transporter adopts outward-facing (C_o), occluded (O_{cc}) and inward-facing (C_i) conformations (Fig. 1), probably among several others. Interconversion between these states facilitates the translocation of the amino acid leucine across bacterial membranes. X-ray crystal structures have been determined for LeuT in the C_o and O_{cc} conformations[9,10], but Zhao *et al.*[4] now bring to light previously unknown features of the conformational cycle of the transporter.

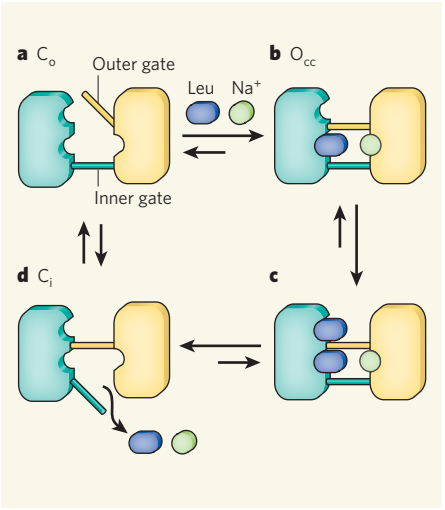

Figure 1 | Conformational states of a membrane transporter. The LeuT protein adopts various conformational states as it transports the amino acid leucine across bacterial cell membranes. It consists of a pore containing two gates — the inner and outer gates. Four conformational states are shown here but the total number of states is unknown. **a**, The transport cycle begins with an outward-facing state, C_o, in which the outer gate is open but the inner gate is closed. **b**, The binding of a leucine molecule and a sodium ion at sites between the gates causes the outer gate to close, generating the occluded state (O_{cc}). **c**, A second leucine molecule can then bind to another site just outside the outer gate. **d**, Next, LeuT opens its inner gate and loses all its substrates to form the inward-facing state, C_i. Closure of the inner gate and opening of the outer gate returns LeuT to the C_o state. Zhao *et al.*[4] have used a fluorescence-based, single-molecule technique to study the transition between the C_i and C_o conformations.

Single-molecule FRET is uniquely suited to probing the functional dynamics of proteins, and has already bridged the gap between the statics and mechanics of protein function[11,12]. The technique involves measuring the distance between fluorescent probes strategically attached at different positions within a protein molecule. In this way, researchers can monitor

the magnitude and time frame of conformational changes for individual molecules within a population. The technique also allows the period of time spent in each observable conformation to be determined. These data are especially powerful when interpreted in the context of high-resolution structural information, such as crystal structures.

By attaching a fluorescent label to the gate on the intracellular side of LeuT, Zhao *et al.*[4] used smFRET to characterize the transition of the transporter to the C_i conformation — something that has not been visualized crystallographically. In the absence of substrate, the authors observed two distinct fluorescent states for LeuT, presumably corresponding to the open and closed states of the inner gate. These data suggest that LeuT switches between the C_i and C_o conformations in a process that is driven partly by random Brownian motion.

Interestingly, when the authors added substrates to their dynamic population of transporters, the inner gates of the transporters closed, probably leading to the formation of the O_{cc} conformation in which a sodium ion and a leucine molecule are bound between the two closed gates (Fig. 1). By contrast, when Zhao *et al.* performed smFRET on mutants of LeuT in which the packing of the inner gate is disrupted, they observed that the transporter preferentially adopted the C_i conformation, and that substrate binding no longer closed the gate. By correlating their smFRET data with molecular-dynamics simulations of the inner-gate opening, the authors identified the rotation of a particular transmembrane helix in LeuT as being pivotal to the transporter's conformational transition to the C_i state.

The authors also attached fluorescent labels to the extracellular surface of LeuT to probe the conformation of the outer gate. They observed that the outer gate was closed in the LeuT mutants that were biased towards the C_i state. Conversely, if the outer gate was forced open, then the inner gate closed. The closing of the inner gate is therefore coupled to the opening of the outer gate, suggesting long-distance coupling across the membrane between the two gates in the transporter.

So what next? Zhao *et al.* performed their experiments in detergent solution, but the activities of membrane transporters in natural situations depend on their lipid-bilayer environment. Future single-molecule work on these transporters should therefore be performed in lipid membranes. Furthermore, the authors have reported only a limited part of the transport cycle of LeuT, characterizing the motion of a few helices, rather than the movement of the whole protein. The next step will be to characterize the entire transport cycle. In particular, it will be exciting to see how the binding of substrate to a second leucine-binding site, recently identified[13] above the extracellular outer gate in LeuT, triggers the opening of the inner gate to allow substrate to be released into the cytoplasm. A complete mechanistic description of a transport cycle also requires the identification of all the conformational states and the thermodynamic and kinetic relationships between them. Zhao and colleagues' smFRET study[4] lifts the curtain and shines a spotlight onto some of the choreography of LeuT — but now the audience is waiting to see the entire dance. ■

Nathan K. Karpowich and Da-Neng Wang are at the Kimmel Center for Biology and Medicine at the Skirball Institute of Biomolecular Medicine, and the Department of Cell Biology, New York University School of Medicine, New York, New York 10016, USA.
e-mails: karpowic@saturn.med.nyu.edu; wang@saturn.med.nyu.edu

1. Neher, E. & Sakmann, B. *Nature* **260,** 799–802 (1976).
2. Kang, T. M. & Hilgemann, D. W. *Nature* **427,** 544–548 (2004).
3. Majumdar, D. S. *et al. Proc. Natl Acad. Sci. USA* **104,** 12640–12645 (2007).
4. Zhao, Y. *et al. Nature* **465,** 188–193 (2010).
5. Maloney, P. C. & Wilson, T. H. *Soc. Gen. Physiol. Ser.* **48,** 147–160 (1993).
6. Huang, Y., Lemieux, M. J., Song, J., Auer, M. & Wang, D.-N. *Science* **301,** 616–620 (2003).
7. Abramson, J. *et al. Science* **301,** 610–615 (2003).
8. Law, C. J., Maloney, P. C. & Wang, D.-N. *Annu. Rev. Microbiol.* **62,** 289–305 (2008).
9. Yamashita, A., Singh, S. K., Kawate, T., Jin, Y. & Gouaux, E. *Nature* **437,** 215–223 (2005).
10. Singh, S. K., Piscitelli, C. L., Yamashita, A. & Gouaux, E. *Science* **322,** 1655–1660 (2008).
11. Yasuda, R., Noji, H., Kinosita, K. Jr & Yoshida, M. *Cell* **93,** 1117–1124 (1998).
12. Zhuang, X. *et al. Science* **288,** 2048–2051 (2000).
13. Shi, L., Quick, M., Zhao, Y., Weinstein, H. & Javitch, J. A. *Mol. Cell* **30,** 667–677 (2008).

MATERIALS CHEMISTRY

Controlled nanotube reactions

Maurizio Prato

For many potential applications, carbon nanotubes must be chemically modified, but the reactions involved aren't easily controlled. The discovery of a reversible modification process is a step towards such control.

Striking the right balance between chemical reactivity and selectivity — a measure of the number of unwanted side reactions associated with a desired reaction — is a challenge that chemists have always faced. Nowhere is this more evident than in the chemistry of carbon nanotubes (CNTs). Because of their low reactivity and high stability, harsh reaction conditions are usually required to 'convince' reluctant CNTs to react. But when they do react, it is difficult to control the number of chemical groups that become covalently attached to the carbon skeleton (the degree of functionalization), a property that is crucial for many applications of CNTs.

Writing in *Angewandte Chemie*, Syrgiannis *et al.*[1] describe one possible solution to the problem. They report a simple method by which chemical groups can be controllably attached to CNTs, then removed and even reattached. The same chemical groups or different ones can be used at different stages of the process, and the degree of functionalization can be varied.

CNTs have many desirable characteristics. Their mechanical, electrical, thermal and optical properties make them useful materials for potential applications such as molecular electronics, biochemical sensors and memory elements or as additives in composite materials. Unfortunately, 'naked' CNTs are difficult to handle because they are insoluble in most solvents. They also tend to aggregate into tight bundles, which makes them difficult to process and prevents researchers from studying the properties of individual CNTs. But when suitable chemical groups are attached to CNTs, they become more soluble in organic solvents and even in water. What's more, chemical modification helps prevent tight bundles of CNTs from forming, almost completely separating individual CNTs from each other.

An entire area of research dedicated to the chemistry of CNTs has thus bloomed over the past decade[2]. One of the most important objectives for this field is to control the degree of functionalization, because although chemical modification helps in the processing of CNTs, too much modification can adversely affect their useful properties. For example, a high degree of chemical modification can alter the conductance of CNTs, which decreases substantially upon increasing functionalization[3]. This effect, which is also related to the type of functionalization[4], is particularly important for CNT-based transistors and for electronic applications in general. Conversely, a high degree of functionalization might be required for other potential uses of CNTs, such as drug delivery.

Syrgiannis and colleagues' technique[1] for controlling the extent of chemical modification of CNTs could therefore be extremely useful. The first step of the process (Fig. 1a) is to covalently attach alkyl groups — saturated hydrocarbons — to the side walls of single-walled CNTs (SWCNTs), using a previously reported reaction[5] that provides high yields of functionalized SWCNTs (f-SWCNTs). The authors' innovation[1] is to have made the process reversible by judiciously modifying the reaction conditions. They found that, by treating the f-SWCNTs with sodium or lithium metal